Small Scale Standing-Wave Thermo-Acoustic Engine

Islam Zakaria-Saleh, B.S MAE — Sound and Vibrations Lab (SVL)
Mentors: Dr. Mostafa Nouh & Dr. Jesse Callanan — SP 2021 - SP 2022

Intro

The purpose of this research project was to determine the possibility of converting thermal energy into acoustic work which can be used to generate electricity. The heat generated produces work in the form of sound waves that 'pump' working gas throughout a resonator creating harmonic, oscillating pressure pulses. These pressure pulses can be used to generate electricity with a variety of electromechanical converters.

Linear Alternators are examples of electromechanical converters that can generate an induced voltage from the linear motion of a coil; linear motion resulting from the mechanical energy of the pressure pulses in a resonator. These pressure pulses can create oscillatory linear motion, the energy of which can be captured by the alternator and used to generate electricity.

Resonator System Identification

The first steps of this part were to attempt to characterize the resonator, determining the resonances of the resonator to be used in closed and open-end conditions. On one end was a speaker that produced a sine sweep of frequencies from 50 Hz to 2 kHz. This speaker served the place of the thermoacoustic source and provided the pressure wave.
The first conducted test was the resonator with a closed boundary at x = L and the speaker will be considered an open boundary. Figure 3 shows the test setup used. A microphone was used at the closed end to measure the pressure waves within the tube. Figure 1 shows the test setup utilized for the open-closed end condition test.

Figure 1: Open/Closed Resonator Setup

A resonator with open and closed-end conditions should exhibit resonance frequencies as shown in equation 1. Where n is the order of the resonance, i.e. first, second, third, and so on resonances.

$$f = \frac{cn}{4L}, n = 1,2,3, \ldots \qquad (1)$$

Figure 2 shows a bode plot showing the transfer function of the voltage measured from the microphone relative to the input speaker voltage; it shows the measured and theoretical resonance magnitude and phase as a function of frequency. The speaker is assumed to be in a near open condition due to the nonperfect seal on the end of the resonator. This can be verified by the body plot; if the experimental and theoretical resonances match closely this assumption can be considered valid.

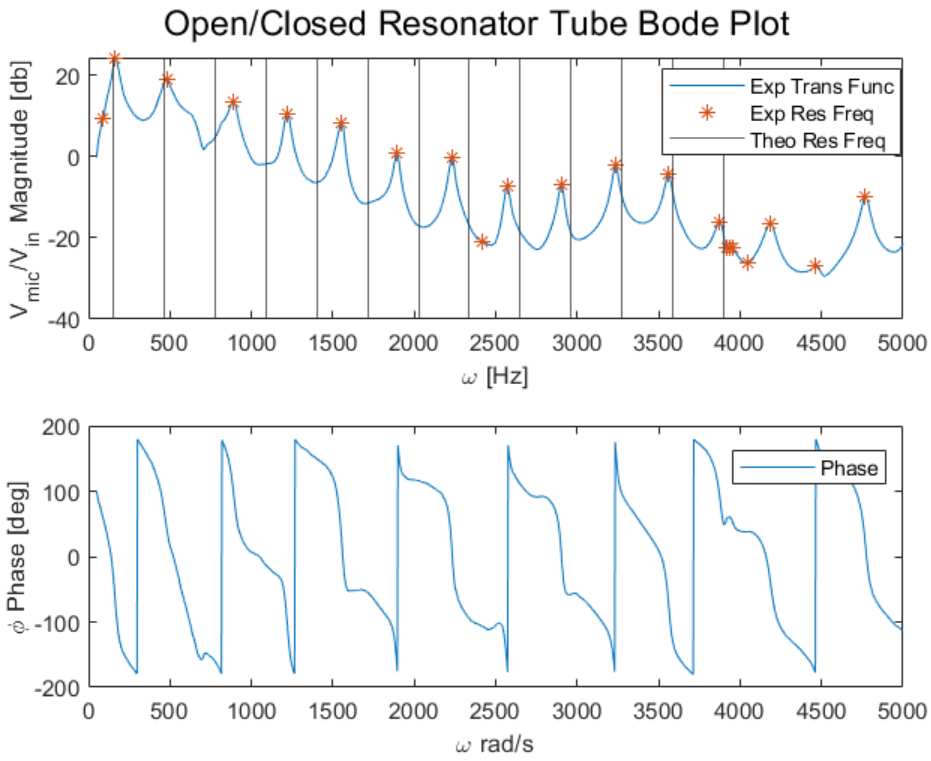

Figure 2: Resonator Bode Plot Open/Closed Condition

Using a resonator length of roughly 0.6 m, the theoretical resonances match very closely to the measured values for the first two resonances, only varying by 10 Hz on average. However, as seen in figure 1 the measured and theoretical resonances no longer match. This means that the assumption that the speaker is an open boundary is reasonable for the first two resonances of the system. Therefore, for any work done at the first two resonances these values can be considered the closed condition limit. These two resonances correspond with an infinite impedance at x = L.

The next step is to determine the upper limit first and second resonances of this tube which corresponds to an open-end condition at x = L, meaning the end impedance is zero. A similar setup was used as in the closed-end condition however the tube is open at the end. In order to measure the resonance frequencies, an accelerometer was attached to the tube to measure the vibration magnitude over a range of frequencies. A resonator with a varying pressure wave in an open/open end condition would have natural resonances at the frequencies described in equation 2.

$$f = \frac{cn}{2L};\ n = 1,2,3,\ldots \tag{2}$$

Figure 3 shows the bode plot of the transfer function related to measured output accelerometer voltage to input speaker voltage. The bode plot also shows the theoretical resonances.

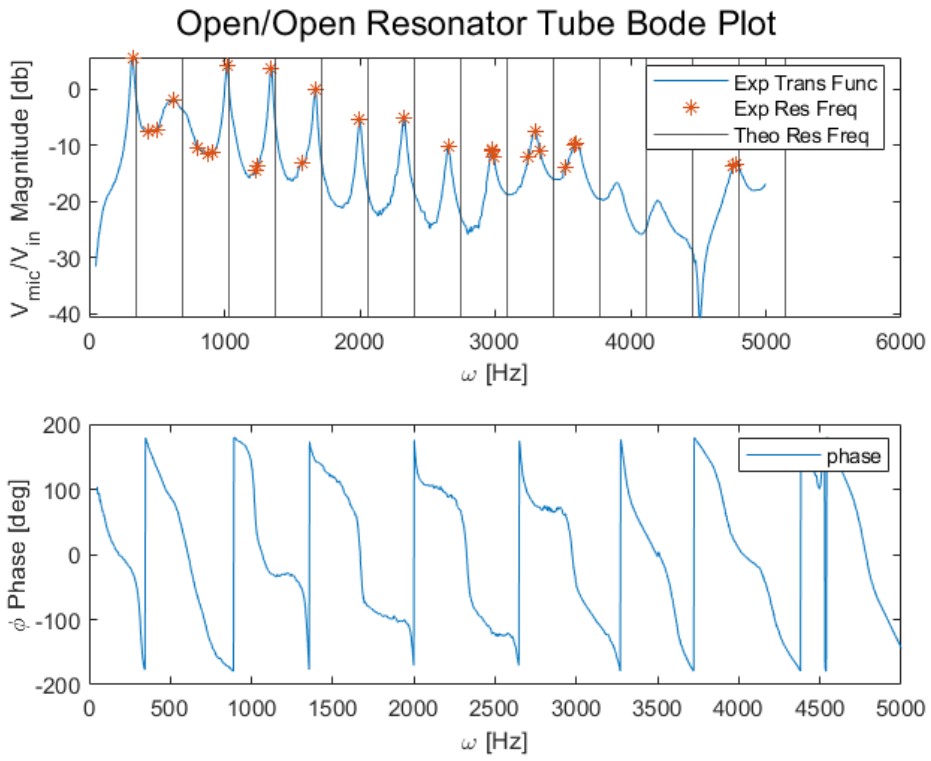

Figure 3: Resonator Bode Plot Open/Open Condition

As seen, the experimental results align quite well with the theoretical resonances, on average varying by about 19 Hz on average for the first four resonances. Now that the resonator can be characterized and the assumption that the speaker is open more valid, I then proceeded to build a linear alternator and begin testing it.

These two tests give a bound of resonances that this system can resonate at. The closed condition represents an infinite impedance boundary meaning the lowest possible resonance and the open represents a zero-impedance representing the highest possible resonance. This means that any finite impedance end condition such as an electromechanical transducer would cause the resonator to resonate at frequencies between the two limits. Table 1 shows the limits for the first two resonances.

Table 1: Resonator Resonances at Different End Conditions

	Closed, $Z = \infty$	**Open, $Z = 0$**	**Intermediate, $\infty < Z < 0$**
First Resonance (Hz)	165	320	(165, 320)
Second Resonance (Hz)	330	640	(330, 640)
Third Resonance (Hz)	479	1017	(479, 1017)

Impedance Matching

In order to get an efficient energy harvester for the thermoacoustic engine, impedance matching between the acoustic impedance of the resonator and the mechanical impedance of the linear alternator was used to determine if the matched impedance frequency is reasonable. By the maximum power transfer theorem, in order to transfer maximum power from an input source, in this case, the acoustic power, to a load which in this case is the alternator, the impedance of the source and load should match. The source acoustic impedance, Z_A, is defined as the ratio of pressure, to particle velocity. The load mechanical impedance, Z_m, is the ratio of acoustic force to coil velocity. In this section, the mathematical model used to determine the acoustic and mechanical impedance of the source and load respectively will be explained.

Acoustic Resonator Description

The thermoacoustic engine consists of a thermal source that causes resonance in a resonator tube. This resonance cause air motion within the tube and this moving air has an associated pressure. The pressure within the resonator tube can be written mathematically in a 1-dimensional approximation of longitudinal waves as a function of time and space shown in equation 3.

$$P(x,t) = Ae^{j(\omega t - k_w x)} + Be^{j(\omega t + k_w x)} \quad (3)$$

This equation consists of two terms; the first represents the forward propagating wave and the second represents the backward propagating wave.

We can also represent the velocity of the fluid, in this case, air, in this resonator. Characterizing both the pressure and velocity of the air in the resonator will better allow us to characterize the entire system and best optimize our engine for the best energy efficiency through methods such as impedance matching with the linear alternator.

Equation 3 describes the velocity of the air as a function of time and space and similarly to the pressure equation it consists of two terms representing the forward and backward propagating waves respectively. Equation 4 is derived from equation 3 and the linearized 1-D Euler equation.

$$U(x,t) = \frac{1}{\rho_0 c}[Ae^{j(\omega t - k_w x)} - Be^{j(\omega t + k_w x)}] \quad (4)$$

Knowing the velocity and pressure at any point within the resonator, the acoustic impedance can be determined. The constants A and B are unknown and require boundary conditions to solve for. If the boundary condition at the beginning of the tube is assumed to be a rigid closed boundary, the air velocity must be zero, in other terms, at x = 0, U(0,t) = 0. This boundary condition results in the constants A and B being equal, resulting in equations 5 and 6 representing P(x,t) and U(x,t) respectively. In each equation the brackets represent P(x) and U(x), and the factored term represents the transience of the pressure and velocity.

$$P(x,t) = Ae^{j\omega t}\left[e^{-jkx} + e^{-jkx}\right] \quad (5)$$

$$U(x,t) = \frac{Ae^{j\omega t}}{\rho_0 c}\left[e^{-jkx} + e^{-jkx}\right] \quad (6)$$

Using these simplified forms, the acoustic impedance of the thermoacoustic engine can be determined by dividing the force by the velocity.

$$Z_A = \frac{4P}{U\pi d^2} = -\frac{4\rho_0 c}{\pi d^2}\frac{\left[e^{-jkx}+e^{-jkx}\right]}{\left[e^{-jkx}+e^{-jkx}\right]} = -\frac{4jc\rho_0}{\pi d^2}\cot\left(\frac{\omega L}{c} + j\alpha L\right) \quad (7)$$

Electromagnetic System Description

A linear alternator is meant to act as an electromechanical transducer that converts mechanical linear motion into a usable voltage. The mini-thermoacoustic linear alternator (MTALA) consists of a coil wrapped around a piston moving through a ring magnet. A coil moving interacting with a changing magnetic field induces a voltage within the coil. Faraday's Law relates the induced voltage, V_i, in the coil to be proportional to the time rate of change of magnetic flux, Φ, through the coil and the number of coils turns N_r as shown in equation 8.

$$V_i = N_r \frac{d\phi}{dt} \tag{8}$$

In a 1-D simplification of a linear alternator the induced voltage in a coil subject to a moving magnetic field can be described as a function of the linear velocity of the coil. The induced voltage in the coil to the velocity via the proportionality constant b that represents many metrics relating to the coil as shown in Equation 9.

$$V_i = b\dot{x}, b = 2\pi N_r r_c \beta \tag{9}$$

This coil can be described as a RLC circuit in series with the induced AC voltage, shown in Fig 4.

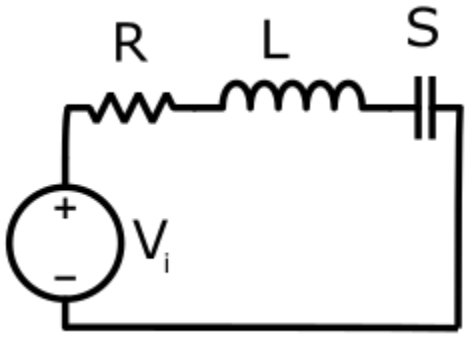

Figure 4: Alternator RLC Circuit

As per Kirchhoff's Voltage law, equation 10 represents the voltage equation of this alternator circuit.

$$V_i(t) = R\dot{q} + L\ddot{q} + Sq \tag{10}$$

Transferring this state equation into the frequency domain as seen in equation 11 below.

$$b\dot{X} = Q[-L\omega^2 + Rj\omega + S] \tag{11}$$

Equation 11 will used to determine the mechanical impedance of the linear alternator.

The mechanical side of this alternator the system can be described as a spring mass damper system. The diaphragm acts as a spring whereas the effects of the magnet act as a damper. Fig 2 shows this simplification.

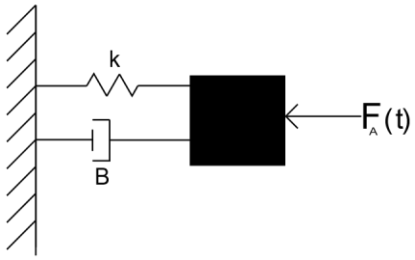

Figure 5: Spring Mass Damper Diagram of Linear Alternator

The equation of motion for the spring mass damper system is shown in equation 12.

$$f_A = m\ddot{x} + c\dot{x} + kx + b\dot{q} \tag{12}$$

Equation 12 can then be transferred to the frequency domain by taking the Laplace transform of the equation. Doing this results in equation 13.

$$\dot{X}(\omega) = j\omega x, \quad F_A = [\dot{X}mj\omega + \dot{X}c + \frac{\dot{X}k}{j\omega} + bj\omega Q] \tag{13}$$

Using equation 6 and substituting equation 13 into it we can then re arrange and determine the mechanical impedance of the electromechanical system of the linear alternator.

$$Z_m = \frac{F_A}{\dot{X}} = mj\omega + c + \frac{k}{j\omega} + \frac{b^2 j\omega}{-L\omega^2 + Rj\omega + \frac{S}{j\omega}} \tag{14}$$

Having the impedance equations for both the mechanical impedance of the alternator and the acoustic impedance of the resonator, we can conduct impedance matching using the fact that at

x = L, $Z_m = Z_A$.

$$mj\omega + c + \frac{k}{j\omega} + \frac{b^2 j\omega}{-L\omega^2 + Rj\omega + \frac{S}{j\omega}} = -\frac{4jc\rho_0}{\pi d^2}\cot(\frac{\omega L}{c} + j\alpha L) \tag{15}$$

Using equation 15, the frequency that results in the highest-pressure force and coil velocity would result in the greatest output voltage.

The electrical and mechanical portion of the linear alternator will each have resonance frequencies. In order to get maximum power transfer, the linear alternator must be modeled such that its resonance frequency closely matches the frequency of the resonator with a finite impedance end condition at $x = L$. The impedance matching method will return a frequency at which the coupled system would resonate. The next step is to vary parameters of the alternator to get matching resonance frequencies.

The resonance of an RLC circuit is defined as the frequency at which electrical impedance is minimized. Using this condition, the resonance of an RLC circuit can be defined with equation 16.

$$f = \frac{n}{2\pi\sqrt{LS}}, n = 1,2,3,\ldots \tag{16}$$

The resonance of a spring mass system is defined using equation 17.

$$f = \frac{n}{2\pi}\sqrt{\frac{k}{m}}, n = 1,2,3,\ldots \tag{17}$$

An electromechanical transducer can be designed such that the electrical and mechanical resonances match with each other and the resonator tube under a finite impedance end condition.

Linear Alternator Design

The initial linear alternator design consisted of a coil attached to two diaphragms at each end mad of elastic material stretched over a circular cross section. Each diaphragm was attached to a cylindrical adapter that allowed the entire system to attach to the resonator tube. Figure 6 shows a cross sectional view of the linear alternator and figure 7 shows the built linear alternator.

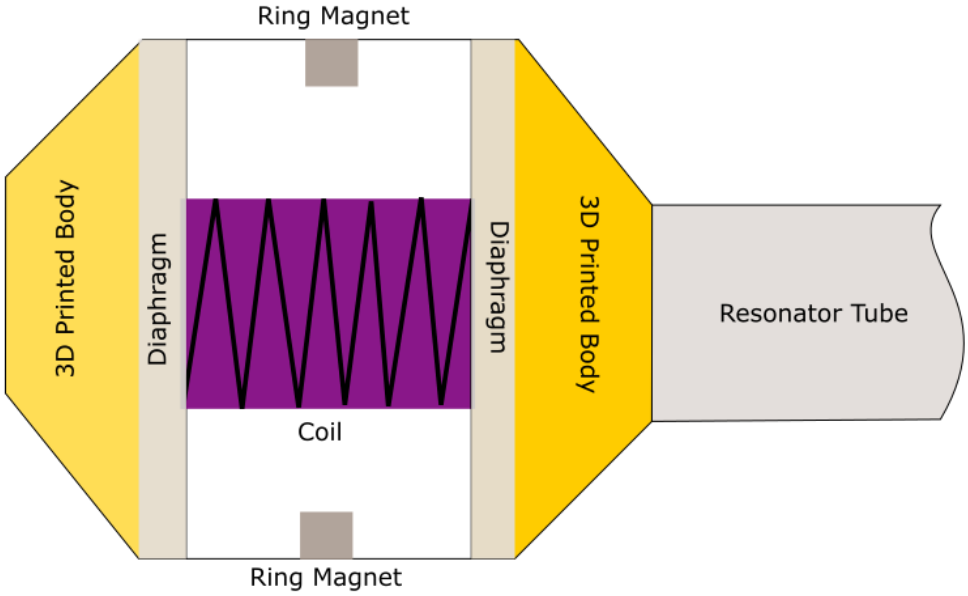

Figure 6: Linear Alternator Cross Section View

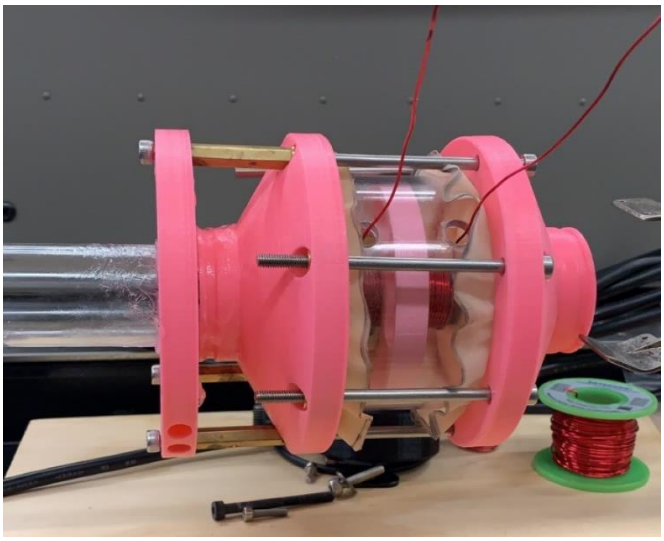

Figure 7: Linear Alternator

Certain parameters of this linear alternator could be modified to optimize the design for energy output. The goal of this alternator is to harvest energy and be made with readily available material at the lab. Some parameters that could affect the performance of the linear alternator involve the resistance, inductance, and weight of the coil. All of these parameters effect the resonance of the alternator as well as its impedance. The mass specifically also effects the structure of the diaphragm; a mass too heavy would deform the diaphragm too much as to not be able to flex at all.

A guiding design parameter for this linear alternator would be the number of turns. As per Faraday's Law, increasing the number of turns on a coil being subject to a changing magnetic field will increase the induced voltage in the coil. However, increasing the number of turns results in a higher piston mass; a heavier piston needs more acoustic power in order to move it. Figure 8 shows how varying tube length and coil turns effects the resonant frequency of the system.

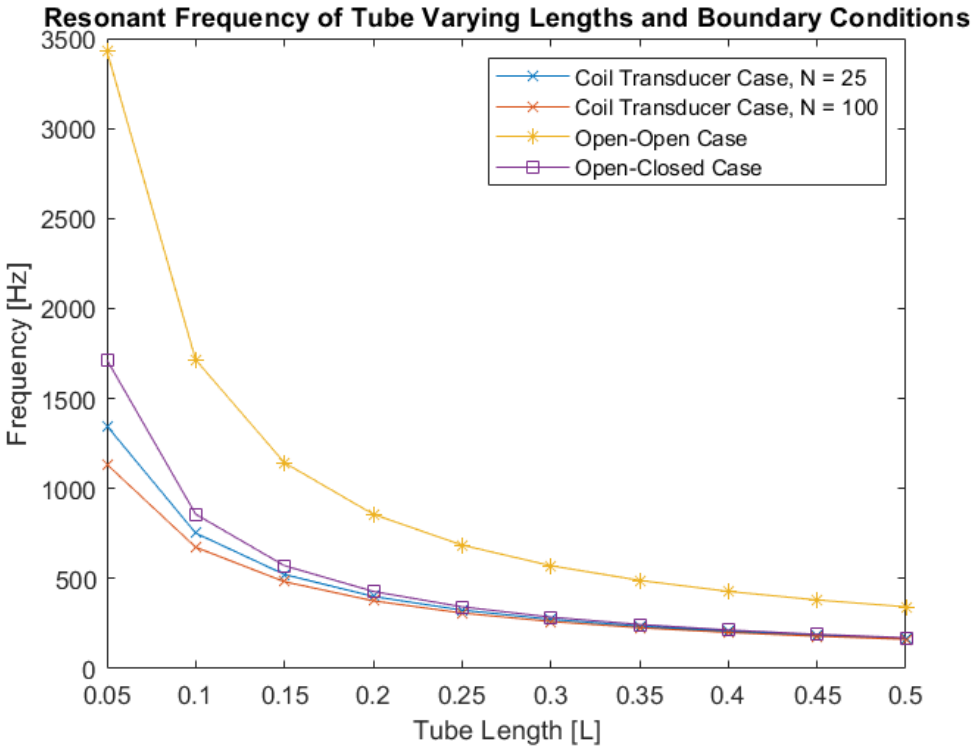

Figure 8: Effect of N_r and L on First Resonance

As seen in figure 8, increasing the number of coils and the length of the resonator decreases the first resonant frequency. However, this plot also shows that varying number of coils turns has a quickly diminishing change of resonant frequency. However, as seen in figure 8, the change diminishes around 0.3 so increasing the length over 0.5 may not change the first resonance much at all regardless of the number of turns on the coil.

In order to describe the linear alternator a plant function can be derived with the input being the acoustic force on the diaphragm and the output is the induced voltage in the coil. The transfer function is shown in equation 18. Equation 18 can be derived from equation 14 for the mechanical impedance of the linear alternator by multiplying the frequency domain form of the coil linear velocity by the faraday's proportionality constant b.

$$G(s) = \frac{V_i}{F_A} = \frac{b\dot{X}}{F_A} = \frac{b(Ls^2+Rs)}{Lms^3+Rms^2+(b^2+kL)s+kR} \tag{18}$$

The inductance, resistance, and mass terms in this transfer functions can all be described as functions of the coil parameters such as gauge and number of turns. These coil parameters can have a direct influence on the mechanical impedance of the linear alternator. Ideally minimizing the impedance can help the transducer better preform practically since it is easier to get the engine to onset in a closer to open end condition as opposed to the closed condition. The wire gauge of the coil directly effects the diameter of the coil in turn effecting its weight as well as its electrical inductance and resistance. These factors can in turn change the mechanical and electrical impedance of the alternator. Figure 9 shows how both mechanical and electrical impedance changes as a function of wire gauge.

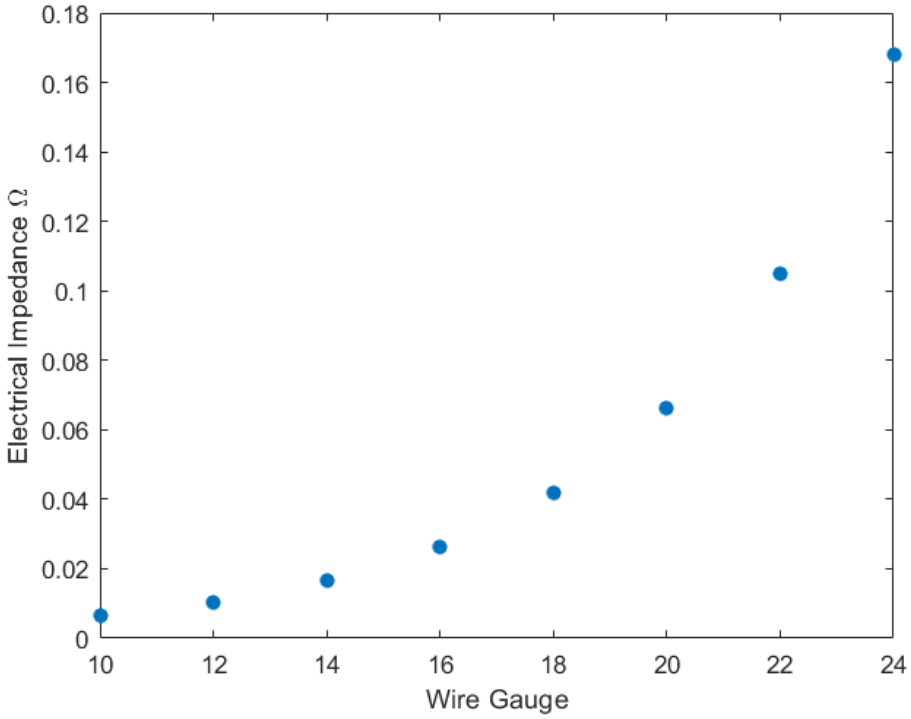

Figure 9: Coil Electrical Impedance vs Wire Gauge

As seen in the figure 9 the electrical impedance increases almost exponentially as wire gauge increases this is due to resistance per length and inductance increasing as diameter of wire decreases.

Therefore, the magnitude of G(s) can be plotted as a function of N_r and an optimum N_r can be selected. Figure 10 shows this plot. It is to be noted that other properties of the coil were kept constant i.e. wire density, wire gauge, and wire resistance per unit length.

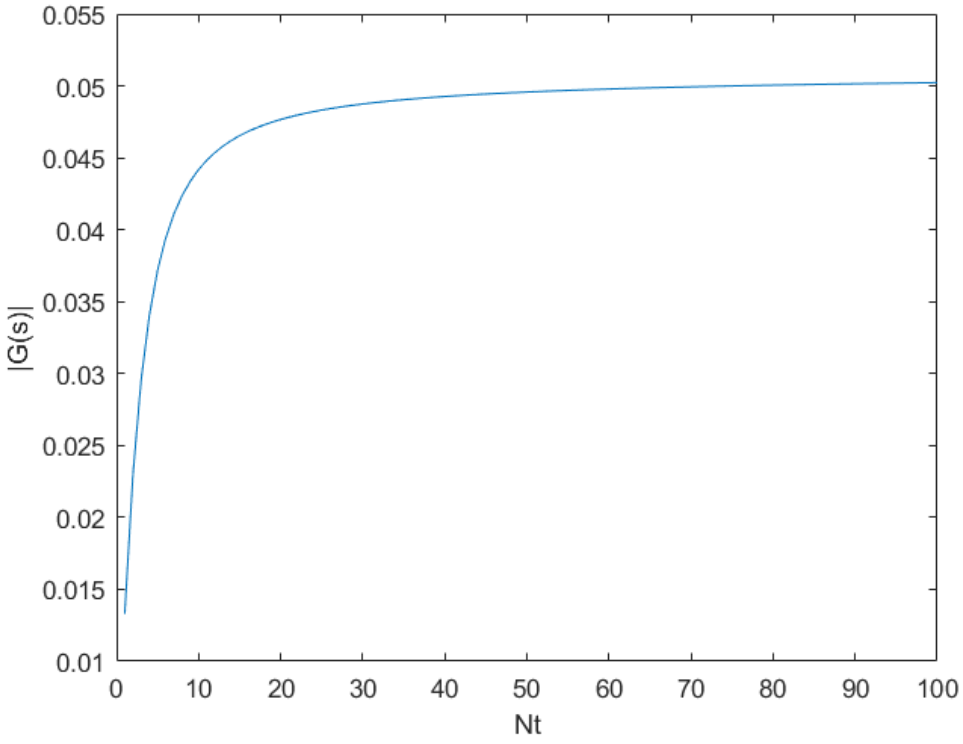

Figure 10: Coil N_r effect on magnitude of plant function

As seen in figure 9, the optimum number of 22-gauge copper wire for this design of linear alternator would be roughly around 20-25 turns. This optimizes the voltage relative to force for the linear alternator. This same method can be modified for a different alternator/speaker design.

The next step in this process was to test the linear alternator under a constant actuating force via an electrodynamic shaker. A sine sweep test was ran in order to generate a transfer function for the alternator under the shaker's actuation force. Figure 10 depicts the generated transfer function.

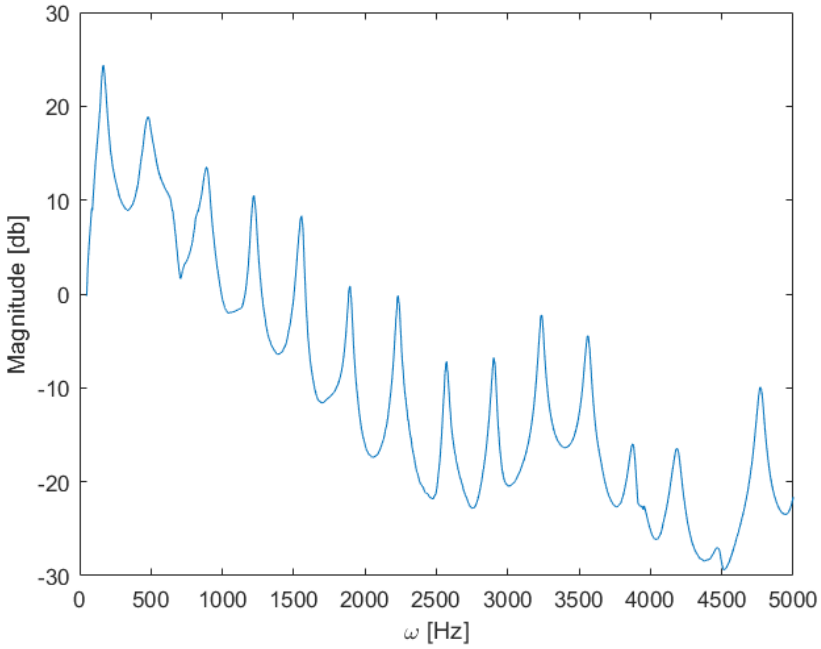

Figure 11: Alternator Attached to Shaker Magnitude Plot

Figure 10, portrays the bode magnitude plot of the resonator tube coupled with the alternator with the speaker being the acoustic source. The plot shows evenly spaced resonance frequencies; each resonance frequency is spaced about 327 Hz apart, with the first resonance at 167 Hz. This first peak can be compared to the transfer function given in equation 18, this can verify if the determined transfer function is accurate enough to model a linear alternator/speaker.

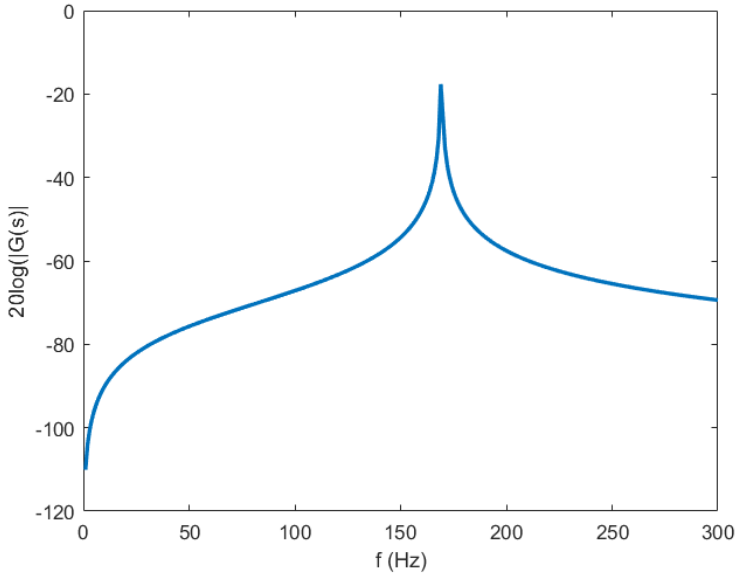

Figure 12: G(s) Magnitude Plot

Figure 11 shows the first resonance of the transfer function and shows a resonance peak at 169 Hz which is very close to the measured resonance at 167 Hz from the shaker test. This shows that the model is relatively accurate within the assumptions made.

Theoretical Predictions and Linear Alternators Results

After optimizing the alternator, the next step was to attach it to a thermoacoustic source and resonator of the same length. Figure 12 below shows the entire system.

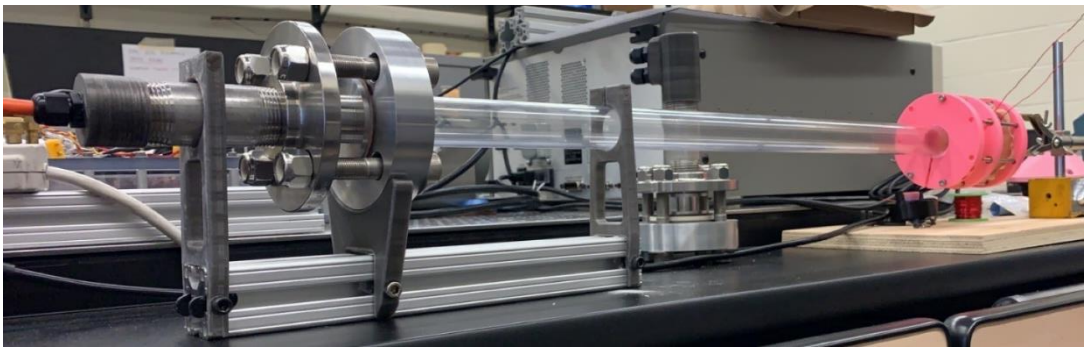

Figure 13: Complete Thermoacoustic Engine

In order to theoretically predict the output voltage of the linear alternator can be determined by equation 9 where the b parameter is known and a function of linear alternator properties. By attaching an accelerometer to the coil, the linear acceleration of the coil can be measured and the velocity of the coils can be acquired. With the velocity and the Faraday parameter a theoretical voltage can be determined. Figure 13 shows a FFT plot of the accelerometer data as well as a the transient plot of the voltage measured by the accelerometer. The FFT shows the first resonant frequency of the combined system is roughly 130 Hz for a slightly longer length of roughly 0.75 m.

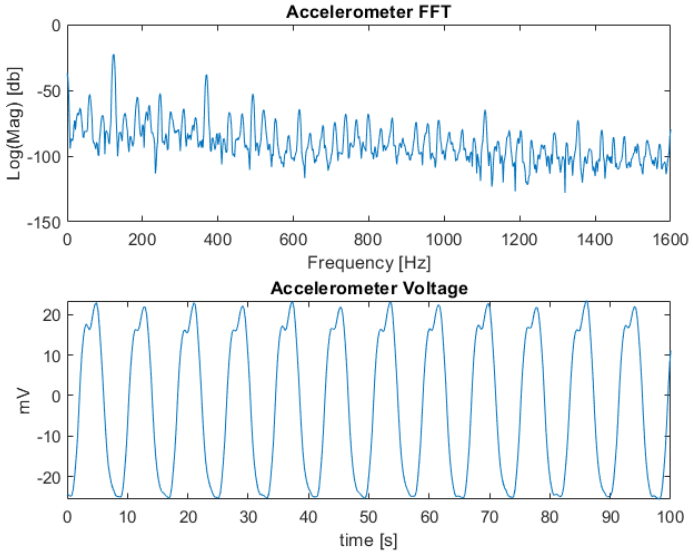

Figure 14: Accelerometer FFT and Transient Voltage Data Plot

Using the sensitivity of the accelerometer the acceleration of the coil can be determined. A function was fitted to the acceleration data shown in equation 19. Figure 14 shows the accelerometer data and the fitted curve.

$$a(t) = -Acos(wt + \phi) = -2.6137cos(0.7799t + 0.3363) \quad (19)$$

This function can then be integrated to get velocity assuming an initial condition of zero velocity at the start. Equation 20 shows the velocity of the coil and equation 21 shows the voltage induced.

$$v(t) = -\frac{A}{w}sin(wt + \phi) = -3.3514sin(0.7799t + 0.3363) \quad (20)$$

$$V(t) = bv(t) = -0.0526sin(0.7799t + 0.3363) \quad (21)$$

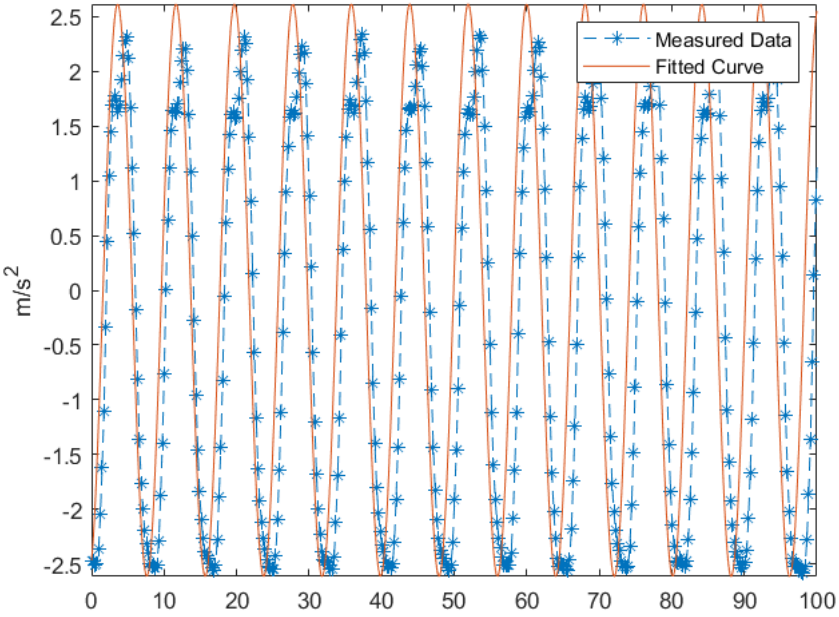

Figure 15: Accelerometer Data and Acceleration Fit Function

As seen in figure 14 the fitted function fits the acceleration data relatively closely with the only issue with the fit is the peak on the positive phase of the signal does not match exactly since the signal is not a perfect sinewave with a higher freedom in one direction due to manufacturing and design.

Figure 15 below shows the calculated fit velocity and the theoretical output voltage of this system.

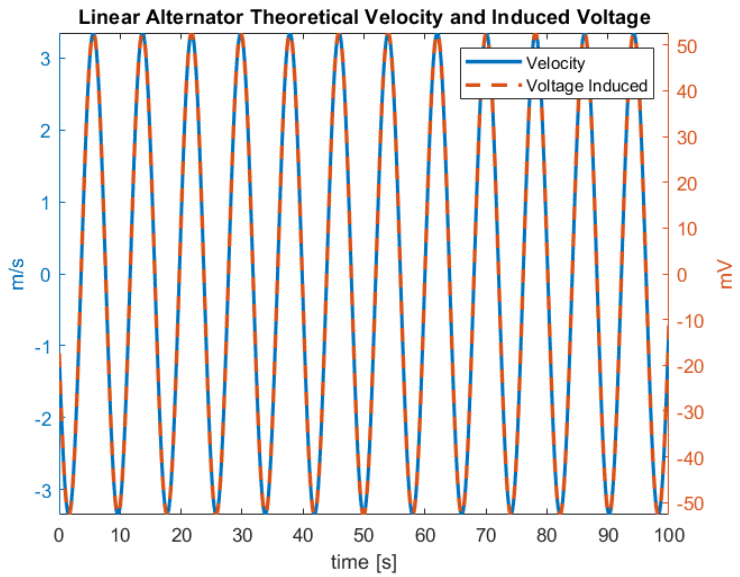

Figure 16: Linear Alternator Transient Velocity and Voltage

Seeing that the theoretical voltage as is was so little it was decided that the use of a commercial speaker would prove to be much more efficient than a 'home made' electromechanical transducer due to limitations in manufacturing and materials. The linear alternator was prone to leaks, stopping the system from oscillating at high magnitudes diminishing the voltage induced in the coil.

Commercial Speaker as a Linear Alternator

Due to limitations in materials and prototyping capability a commercial 4-ohm speaker was used as an electromechanical transducer. The speaker was attached to the thermoacoustic engine as seen in figure 16.

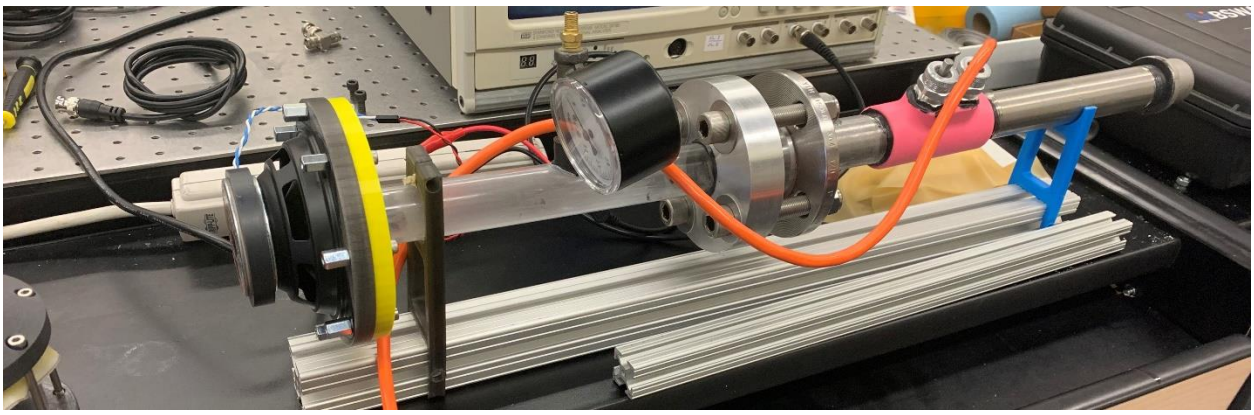

Figure 17: Thermoacoustic Engine with Commercial Speaker

In this configuration the speaker was able to generate an AC voltage relatively higher than the theoretical output of the linear alternator. This configuration allows for the distance between the speaker diaphragm and the outlet of the resonator to be changed. Changing

this distance in turn changes the area of the speaker being pressured by air. Theoretically decreasing this area would increase the force in turn increasing output.

The commercial speaker is attached to a 3D printed adapter that connects to the resonator tube. The speaker was tested in 3 configurations in order to see how the effective cross-sectional area affects electrical output. The effective cross-sectional area is defined as the cross-sectional area on the speaker that the acoustic pressure wave will interact with. In theory, the pressure should stay constant, meaning the as the area decreases the force on the coil increases maker the coil displaces more at a higher acceleration and velocity which directly increases the electrical output. The speaker was tested in 3 configurations: the speaker held close to the outlet but not sealed, meaning the system was completely open, the second involved the speaker with the adapter attached to the resonator 'closing' the tube therefore the system is no longer in an open end condition with an effective cross-sectional diameter equal to the diameter of the speaker rim, and the last was the same as the second but with a cross sectional diameter roughly equal to the resonator.

Figure 18 below shows an FFT, transient voltage output, and rms-voltage output for all three configurations.

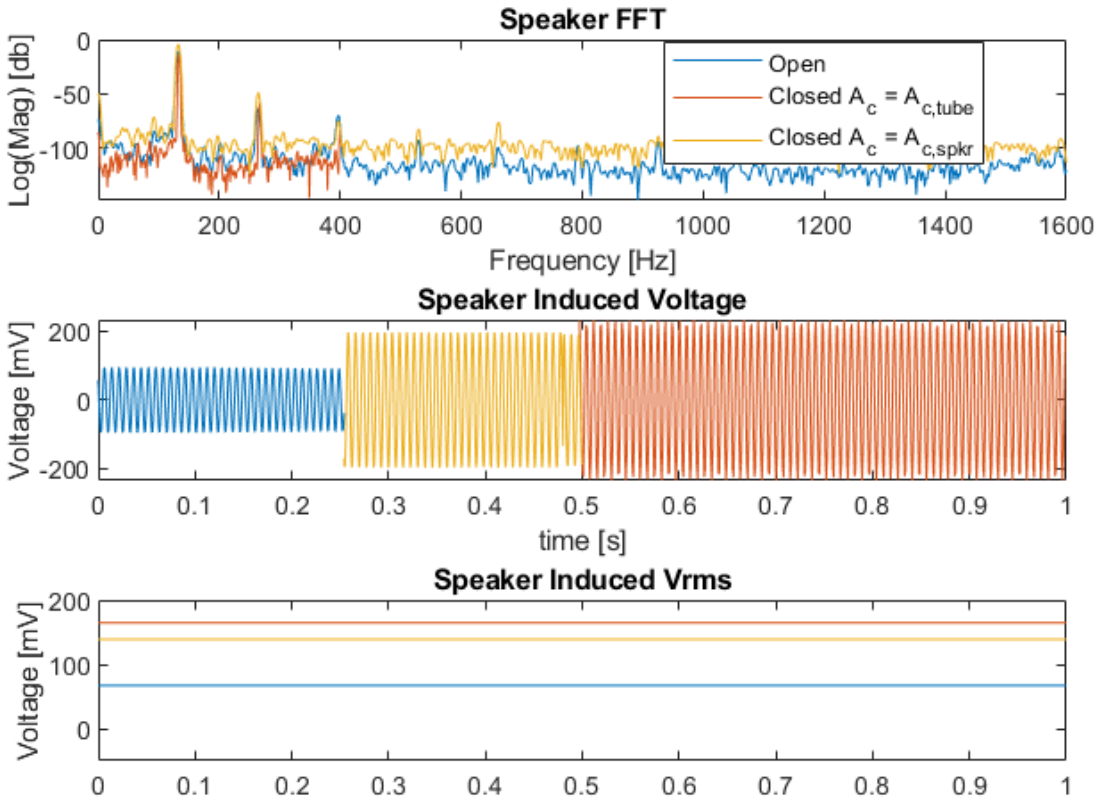

Figure 18: Speaker Data from 3 Configurations

As seen in figure 18, the speaker induced voltage increased by decreasing the effective cross-sectional area for the system. The resonance points remained the same for all three cases roughly around 136 Hz, which is reasonable due to the impedance in each case remaining constant. This data confirms that placing the speaker close enough such that the effective area is roughly the same as the resonator produces the highest output.

The final tests completed for this system involved stack length and its effect on the output of the engine. It's inferred that by increasing the stack length the temperature difference along the stack would be greater, causing more rapid air movement and increasing the amplitude of the acoustic wave. Therefore, increasing the stack length should increase the power output however, this relationship is not necessarily linear. A paper from the third IEEE Eurasia Conference on IOT by Irna Farikhah tested the effect of stack length on the output of a traveling wave thermoacoustic engine. Figure 19 shows how stack length effects output efficiency in a traveling wave engine.

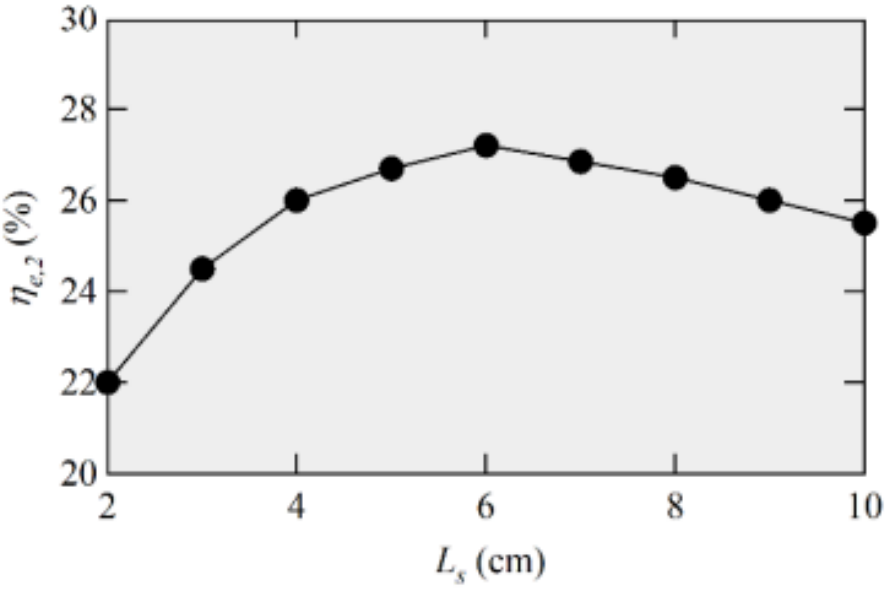

Figure 19: Effect of Stack Length on Traveling Wave Engine Efficiency []

In the configuration used, figure 19 shows that output efficiency is not linearly related to stack length however there seems to be a positive relationship between the two with a point of diminishing returns at roughly 6 cm stack length with a peak efficiency of 27%. With this as a jumping point, the stack of the standing wave engine was changed from 2.5 cm to roughly 5 cm. Figure 20 below shows the change the new speaker output.

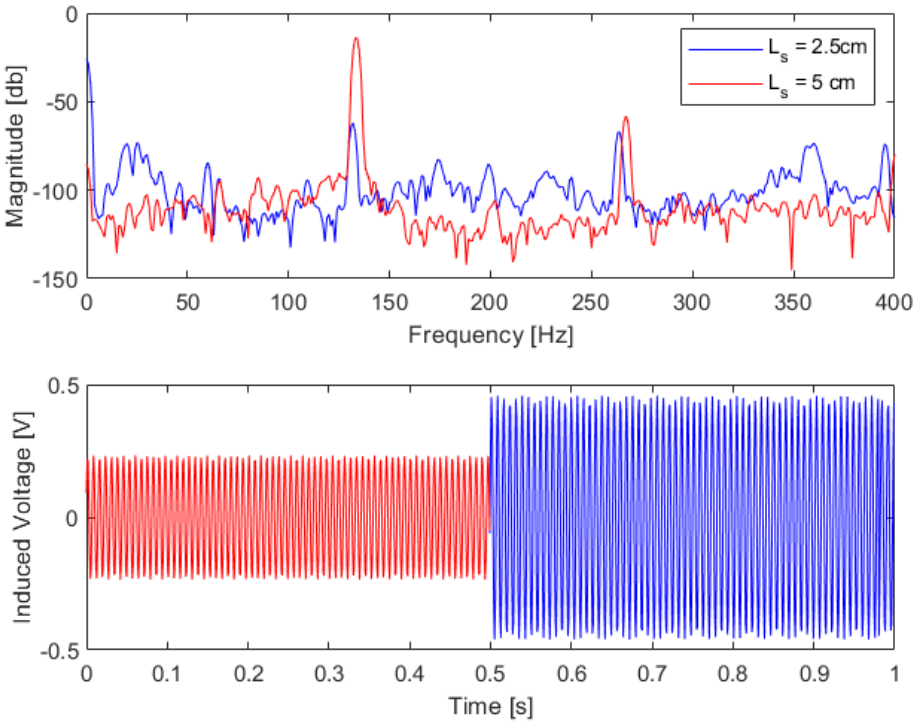

Figure 20: Effect on Stack Length on Engine Output

As seen in figure 20, the 2x increase in stack length resulted in a nearly two times increase in peak voltage from 230 mV to roughly 455 mV. The resonance peak stayed nearly the same only increasing by 3 Hz from 122 Hz to 135 Hz. This data is some evidence that stack length can increase engine efficiency and more study can go into seeing the type relationship between stack length and engine efficiency similar to what is seen in figure 19.

Potential Next Steps for This Project

This project is still far from finished. A big goal for this project would be to attempt to reach a higher efficiency, ideally within the magnitude of at least 10-20%. Many things can go into achieving this such as improving on the build quality focusing on ensuring a proper seal between the alternator and the resonator as leaks reduce the efficiency of the engine. Another task should include better speaker sizing, mainly focusing on selecting a speaker with an operating range of that closer to the engine. The engine with a finite impedance end condition such as a speaker has its first resonance in the range of 100-200 Hz, whereas the 4-ohm speaker used has a resonance closer to 500 Hz. Sizing a speaker closer to 100-200 Hz would drastically increase the output efficiency. Another task could also be looking into how to excite different modes of the engine. By changing the current through the wire and in turn the temperature difference along the stack different modes of the engine can be emphasized as seen in figure 21.

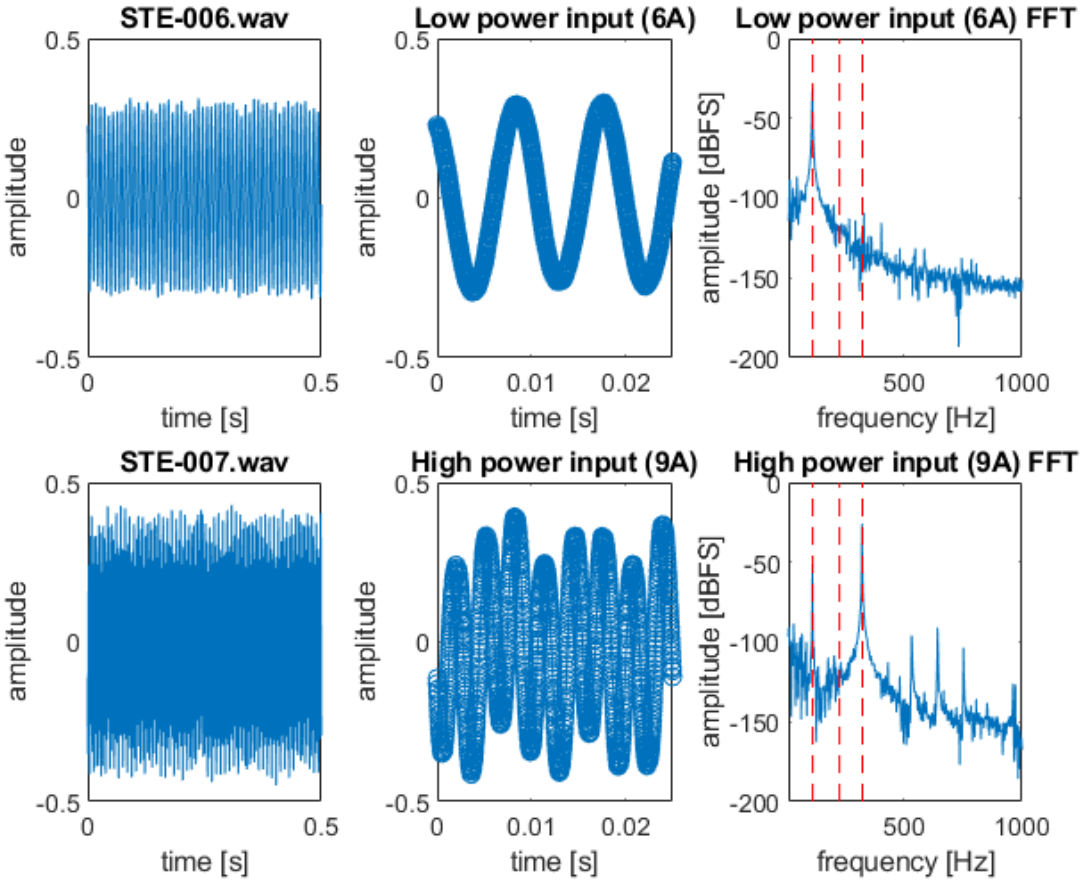

Figure 21: Engine Mode Prominence at Different Power Inputs

As seen in figure 21, by changing the current in the wire from 6 A to 9 A the temperature difference along the stack increased and a higher mode acoustic wave was onset. The top right plot shows that the prominent mode is the first at roughly 120 Hz in this case. In the increased power scenario, the higher 340 Hz mode became more prominent. As opposed to sizing a speaker that operates in the first resonance range of the speaker, potentially by changing the input power to the engine, a higher mode that matches a speaker can be emphasized to increase engine output.

Along with increasing the power output of this small-scale engine more work can be put into using different heat sources for practicality. As of now the heat source to onset the engine is a neo-chrome wire that heats up as current runs through it. However, if this engine were to be used in energy scavenging applications, the heat source should be a naturally occurring heat source. Ideally this engine would onset from waste heat that can be channeled onto the stack to develop the temperature difference. This project can also go into looking at refrigeration, where instead of using a temperature difference to produce energy, one would use energy to induce a temperature difference.

Acknowledgments and Final Remarks

This project has genuinely been an enriching experience for my career as an engineer. I learned a lot over the year, being a part of the Sound and Vibrations Lab at UB. Not, only did I get to learn a lot about thermoacoustic, energy harvesting, and multiphysics problems, I learned a lot about engineering research and the process of theorizing, experimenting, analyzing, and iterating required to produce valuable results. I grew tremendously as an engineer and research thanks to the help from my mentors who guided and taught me how to continue to improve over the course of this project.

I would like to acknowledge the guidance and mentorship provided to me by Dr. Jesse Callanan. He was my main source of guidance and support during this project teaching me a lot about thermoacoustics, how to conduct research, and how work independently on a project and iterate on my work.

I would also like to acknowledge the guidance provided by Dr. Mostafa Nouh, the principal investigator of the Sound and Vibrations Lab. I am grateful to Dr. Nouh for providing me this opportunity to study and work with the lab as well as supporting me and providing guidance to me through out the project and helping me acquire the Zimmer scholarship for undergraduate research.

I would also like to acknowledge the help of PhD candidate in the SVL, Revant Adlakha for his mentorship and guidance on this project. Revant regularly provided me advice and guidance on where to take the project and how to improve on it as well as developing next steps for this project.

Finally, I would like to thank the rest of the Sound and Vibrations Lab for also aiding and supporting me throughout this experience and creating an atmosphere of curiosity, mentorship, and comradery. The members of the SVL have created a culture and environment ripe for learning and growth, continuing to innovate and conduct excellent and world class research.

Refrences

[1] Avent, A. W., & Bowen, C. R.. (2015). Principles of thermoacoustic energy harvesting. *The European Physical Journal Special Topics*, *224*(14-15), 2967–2992. https://doi.org/10.1140/epjst/e2015-02601-x

[2] Geng Chen, Lihua Tang, Brian Mace, Zhibin Yu, Multi-physics coupling in thermoacoustic devices: A review, Renewable and Sustainable Energy Reviews, Volume 146, 2021, 111170, ISSN 1364-0321, https://doi.org/10.1016/j.rser.2021.111170.

[3] Timmer, M. A. G., De Blok, K., & Van Der Meer, T. H.. (2018). Review on the conversion of thermoacoustic power into electricity. *The Journal of the*

Acoustical Society of America, *143*(2), 841–857. https://doi.org/10.1121/1.5023395

[4] J. Smoker, M. Nouh, O. Aldraihem, *and* A. Baz , "Energy harvesting from a standing wave thermoacoustic-piezoelectric resonator", Journal of Applied Physics 111, 104901 (2012) https://doi.org/10.1063/1.4712630

[5] Pillai, M. A., & Deenadayalan, E.. (2014). A review of acoustic energy harvesting. *International Journal of Precision Engineering and Manufacturing*, *15*(5), 949–965. https://doi.org/10.1007/s12541-014-0422-x

[6] M. Nouh, O. Aldraihem, A. Baz, Piezo-driven thermoacoustic refrigerators with dynamic magnifiers, Applied Acoustics, Volume 83, 2014, Pages 86-99, ISSN 0003-682X, https://doi.org/10.1016/j.apacoust.2014.02.017.

[7] Tijani, M. E. H., Zeegers, J. C. H., & De Waele, A. T. A. M.. (2002). Design of thermoacoustic refrigerators. *Cryogenics*, *42*(1), 49–57. https://doi.org/10.1016/s0011-2275(01)00179-5

[8] I. Farikhah *et al.*, "Study of Stack Length on Efficiency of Thermoacoustic Engine," *2021 IEEE 3rd Eurasia Conference on IOT, Communication and Engineering (ECICE)*, 2021, pp. 580-582, doi: 10.1109/ECICE52819.2021.9645691.